Lifetime-based tomographic multiplexing

Citation: Scott B. Raymond, David A. Boas, Brian J. Bacskai and Anand T. N. Kumar, "Lifetime-based tomographic multiplexing", J. Biomed. Opt. 15, 046011 (Aug 06, 2010); doi:10.1117/1.3469797 © 2010 Society of Photo-Optical Instrumentation Engineers

As Published: http://dx.doi.org/10.1117/1.3469797

Publisher: SPIE

Persistent URL: http://hdl.handle.net/1721.1/60943

Version: Final published version: final published article, as it appeared in a journal, conference proceedings, or other formally published context

Lifetime-based tomographic multiplexing

Scott B. Raymond
The Harvard-MIT Division of Health Sciences and Technology
114 16th Street
Charlestown, Massachusetts 02129

David A. Boas
Massachusetts General Hospital
Department of Radiology
Athinoula A. Martinos Center for Biomedical Imaging
149 13th Street
Charlestown, Massachusetts 02129

Brian J. Bacskai
Massachusetts General Hospital
Department of Neurology
Alzheimer's Research Unit
114 16th Street
Charlestown, Massachusetts 02129

Anand T. N. Kumar
Massachusetts General Hospital
Department of Radiology
Athinoula A. Martinos Center for Biomedical Imaging
149 13th Street
Charlestown, Massachusetts 02129

Abstract. Near-infrared (NIR) fluorescence tomography of multiple fluorophores has previously been limited by the bandwidth of the NIR spectral regime and the broad emission spectra of most NIR fluorophores. We describe *in vivo* tomography of three spectrally overlapping fluorophores using fluorescence lifetime-based separation. Time-domain images are acquired using a voltage-gated, intensified charge-coupled device (CCD) in free-space transmission geometry with 750 nm Ti:sapphire laser excitation. Lifetime components are fit from the asymptotic portion of fluorescence decay curve and reconstructed separately with a lifetime-adjusted forward model. We use this system to test the *in vivo* lifetime multiplexing suitability of commercially available fluorophores, and demonstrate lifetime multiplexing in solution mixtures and in nude mice. All of the fluorophores tested exhibit nearly monoexponential decays, with narrow *in vivo* lifetime distributions suitable for lifetime multiplexing. Quantitative separation of two fluorophores with lifetimes of 1.1 and 1.37 ns is demonstrated for relative concentrations of 1:5. Finally, we demonstrate tomographic imaging of two and three fluorophores in nude mice with fluorophores that localize to distinct organ systems. This technique should be widely applicable to imaging multiple NIR fluorophores in 3-D.
 [DOI: 10.1117/1.3469797]

Keywords: near-infrared fluorescence; tomography; lifetime; small animal imaging.

Paper 10147R received Mar. 21, 2010; revised manuscript received May 16, 2010; accepted for publication Jun. 1, 2010; published online Aug. 6, 2010.

1 Introduction

The ability to image multiple fluorophores simultaneously (multiplexing) in the visible regime (350 to 700 nm) has been critical for understanding a variety of biological processes.[1–4] Conventionally, multiplexing is achieved using fluorophores with different emission wavelengths and filtering the combined emission into multiple channels, or by postprocessing a spectral measurement to unmix the combined signals. These techniques have been widely adopted for visible fluorescence imaging at the microscopic and whole-animal levels.

In the NIR spectral regime (700 to 900 nm), imaging has traditionally been performed on one to two fluorophores. Limited bandwidth and the highly overlapping spectra of most commercial NIR fluorophores make it difficult to resolve more than two probes at once without sophisticated unmixing algorithms. Near-infrared fluorescence (NIRF) tomography is further complicated by the differential effects of tissue absorption for a multiwavelength measurement.[5] Fluorescence lifetime is an identifying characteristic, separate from the emission spectrum, that can be used to distinguish fluorophores.[6] We have developed a methodology for NIRF tomographic multiplexing using characteristic fluorophore lifetimes to separate multiple probes. This approach relies on the fact that fluorophores exhibit a time-resolved decay pattern that can be easily characterized and is very often monoexponential with a decay rate of $1/\tau$. A mixture of n fluorophores, when excited by an impulse, will exhibit time-dependent fluorescence emission $f(t)$ that is a sum of the respective fluorophore decays:

$$f(t) = a_o + a_1 \exp(-t/\tau_1) + a_2 \exp(-t/\tau_2) \ldots + a_n \exp(-t/\tau_n). \quad (1)$$

Although sophisticated numerical methods exist to obtain the amplitudes and lifetimes from a mixture of fluorophores, simplification is achieved in many cases when the lifetimes can be determined experimentally in advance. Assuming known lifetimes $(\tau_1 \ldots \tau_n)$, amplitude components $(a_1 \ldots a_n)$ can be determined by directly fitting $f(t)$.[7,8] Equation (1) provides a simple way to unmix or separate the signal from multiple fluorophores and has been used for surface imaging in a number of recent studies.[8–10] When fluorophores are imaged deep in tissue, i.e., in tomographic measurements, it can be shown that fluorescence decay can be expressed in a form similar to Eq. (1) with slight modifications to account for the time-dependent effects of tissue absorption and scattering.[11]

We present here the first *in vivo* lifetime-multiplexed NIRF tomography based on linear unmixing of the time-domain signal and subsequent tomographic reconstruction of the individual lifetime components. We begin by characterizing the

Address all correspondence to: Anand Kumar, Athinoula A. Martinos Center for Biomedical Imaging, Department of Radiology, Massachusetts General Hospital, 149 13th Street, Charlestown, Massachusetts 02129. Tel: 617-726-8394; Fax: 617-643-5136; E-mail: ankumar@nmr.mgh.harvard.edu

1083-3668/2010/15(4)/046011/9/$25.00 © 2010 SPIE

lifetime behavior of a number of commercially available NIR fluorophores *in vivo* to determine the suitability for lifetime-based multiplexing. We next compare lifetime-based fluorophore multiplexing to traditional monoexponential analysis, and establish the limits of quantitative multiplexing based on imaging system noise parameters and lifetime differences. Finally, we demonstrate tomographic lifetime multiplexing with up to three fluorophores in nude mice.

2 Methods

2.1 *Imaging System*

Time-resolved imaging was performed with a free-space, time-domain, tomographic imaging system described previously.[12] Excitation was provided by a fiber-coupled, femtosecond laser at 700 nm, with ~100-mW average power, 80-MHz repetition rate (Mai Tai, Newport-Spectra Physics, Mountain View, California). Excitation light was either: 1. focused (point source) and scanned across the ventral surface of the animal from below for tomography, or 2. expanded with an engineered diffuser (Thorlabs, Newton, New Jersey), resulting in a ~5×5-cm illumination region at the imaging platform for planar fluorescence imaging. Excitation and emission images were acquired with a cooled CCD camera (Picostar HR-12 CAM 2, LaVision GmbH Goettingen, Germany; 2×2 or 4×4 hardware binning) mounted to a voltage-gated image intensifier (Picostar HR-12, LaVision GmbH, Goettingen, Germany). For all measurements, a background image (with no excitation) was subtracted. Light was focused into the intensifier with a 60-mm lens (AF Nikkor, f2.8, Nikon), and filtered with 2-in. filters mounted directly to the front of the lens (TFI Technologies, Greenfield Massachusetts; Chroma Technology Corporation, Rockingham, Vermont). 3-D boundaries were captured with a photogrammetric camera (3-D Facecam 100, Genex Technologies Incorporated, Kensington, Maryland). Gates were collected every 100 ps for ~10 ns in planar scans and every 200 ps for ~10 ns in tomographic scan. CCD exposure time ranged from 100 to 1000 ms, and the buffer readout time was 230 ms for 4×4 binning, and 450 ms for 2×2 hardware binning. A typical planar scan with 500-ms exposure and 80 frames (taken every 100 ps) took 1 min to acquire. A typical tomographic scan imaged at 52 source positions for 9 ns in steps of 0.2 ns (46 gates) with 100-ms exposure took 13 min., including the excitation and 3-D camera measurements. The total tomography acquisition took roughly 30 min.

2.2 *Asymptotic Lifetime Fitting*

Lifetime analysis was performed in the "asymptotic" regime, defined as the portion of the temporal decay where the intrinsic diffuse temporal response has completed its evolution, i.e., for all times greater than the diffuse time constant τ_D.[11] The beginning of the asymptotic time regime $t=\tau_D$ was determined for each source-detector (SD) pair independently by finding the time gate t_D for which the time integral $\int_0^t e^{t'/\tau} U_{\mathrm{exc}}\, dt'$ was at 99% of its maximum value. The rationale behind this approach is that this integral is an approximation of the time-dependent amplitude coefficient for the decay of the particular lifetime τ.[12] Lifetime components were fit according to Eq. (1) for time points $t \geqslant t_D$. The $t=0$ time gate (t_o), which corresponds to the time of incidence of the laser pulse at the boundary of the imaging medium, was determined directly from an excitation measurement taken with sources projected on a piece of white paper in the imaging plane;[12] the time axis for all subsequent measurements and analysis was translated such that $t=0$ for the t_o time gate. We used weighted, nonlinear least squares with non-negative constraints (fit.m in Matlab) to determine amplitude components. Weights were $1/\sigma_y^2$, determined from a quantitative noise model of our system, $\sigma_y^2=\beta\bar{y}+\sigma_r^2$.[13] β was determined experimentally for each of the binning schemes used: 4×4 hardware and 2×2 software binning, 6.53; 2×2 hardware and 4×4 software binning, 8.53; 4×4 hardware and 4×4 software binning, 11.38; and 2×2 hardware and 8×8 software, 15.72.

2.3 *Tomography*

Lifetime-separated tomographic reconstructions used the methods outlined in Refs. 11 and 12. The time-domain fluence $U(\mathbf{r}_s,\mathbf{r}_d,t)$ for n lifetimes was modeled in the asymptotic limit as

$$U(\mathbf{r}_s,\mathbf{r}_d,t)=\sum_n \exp(-t/\tau_n)\int_V d^3\mathbf{r}\,\Theta(\mathbf{r}_s,\mathbf{r}_d)\,\bar{W}_n^B(\mathbf{r}_s,\mathbf{r}_d,\mathbf{r})\,\eta_n(\mathbf{r}). \tag{2}$$

$\bar{W}_n^B(\mathbf{r}_s,\mathbf{r}_d,\mathbf{r})$ is the three point or composite Green's function, calculated at the tissue optical properties and reduced by a factor proportional to the respective lifetime, and $\Theta(\mathbf{r}_s,\mathbf{r}_d)$ is the source-detector scaling coefficient that compensates for free-space propagation from a curved surface. Note that Eq. (2) is similar to Eq. (1), but with the decay amplitudes a_n replaced by the integral over the tomographic weight functions. We accounted for transmission heterogeneities by directly measuring excitation light propagation and reconstructing optical properties with the Fourier components of the TD data.[5] The recovered optical properties were then input into a voxel-based Monte Carlo forward model[14] at ≈1 mm^3 resolution to generate $\bar{W}_n^B$. Θ was calculated by comparing the forward generated fluence U_{exc} with the excitation measurement y_{exc}, i.e., by solving the linear equations $U_{\mathrm{exc}}(\mathbf{r}_s,\mathbf{r}_d)=\Theta(s,d)\,y_{\mathrm{exc}}(\mathbf{r}_s,\mathbf{r}_d)$.[15] Equation (2) was solved for each lifetime component independently, with generalized, weighted linear least squares.[16]

2.4 *In Vivo Evaluation of Near-Infrared Fluorophore Lifetime Characteristics*

A variety of NIR fluorophores (indocyanine green, Akorn, Lake Forrest, Illinois; Osteosense 750 nm, Genhance 750, VisEn Medical, Bedford, Massachusetts; IRDye 800CW, LI-COR Biosciences, Lincoln, Nebraska; Kodak X-Sight 761, Carestream Health, Rochester, New York: Atto 740, Sigma-Aldrich, Saint Louis, Missouri; Alexa 750, Invitrogen, Carlsbad, California) were evaluated for *in vivo* lifetime characteristics. Mice (C57, n=4, Charles River Laboratories, Wilmington, Massachusetts nu/nu, n=1, Foxn1^{nu}, the Jackson Laboratories, Bar Harbor, Maine; NCr-Foxn1^{nu}, n=2, Taconic, Hudson, New York) were anesthetized with 2% isoflurane or avertin (1.3% 2,2,2-tribromoethanol, 0.8% tertpen-

tylalcohol; 250 mg/kg), administered NIRF fluorophores (at 0.1 to 3 mg/kg IV), and imaged in the prone and supine positions with planar fluorescence excitation at time points from 1 min to 24 h after injection, depending on the fluorophore pharmacokinetics. For time points more than 4 h after fluorophore administration, animals were allowed to recover from anesthesia, and then anesthetized again immediately before the later time point. Lifetime histograms were generated by a monoexponential fit of all pixels that had cw intensity at least 10% of the maximum intensity. Following euthanasia, organs were imaged *in situ* and *en bloc* after removal.

2.5 *Multiwell Calibration Experiment*

Osteosense 750 and Kodak X-Sight 761 were prepared at varying concentrations in 5% albumin solution, which has been shown to better approximate *in vivo* lifetime.[17] We filled a 6×6 grid of wells in a 96-well plate with concentrations from 0 to 1000 nM, by steps of 200 nM, resulting in a two-axis gradient of the two probes. The wells were imaged in planar fluorescence mode with 750 excitation and a 790-nm bandpass filter. Amplitude uncertainty s_i was calculated as the root of the diagonal of the covariance matrix of the coefficient estimates, or $[(\mathbf{X}^T\mathbf{X})^{-1}\mathrm{sse}/\mathrm{dfe}]^{1/2}$, where X is the design matrix, sse is the sum of the squared error, and dfe is the degrees of freedom.

2.6 *In Vivo Lifetime Multiplexing*

Nude mice (Foxn1^{nu}, n=1, the Jackson Laboratories, Bar Harbor, Maine; NCr-Foxn1^{nu}, n=2, Taconic, Hudson, New York) were administered Osteosense 750 (2 nmols, 24 h before imaging) and Kodak X-Sight (3 nmol per mouse, 1 h before imaging) by tail-vein injection. For three fluorophore experiments, nude mice (n=3, NCr-Foxn1^{nu}, Taconic, Hudson, New York) received Osteosense 750 (2 nmol, >24 h prior to imaging), Atto 740 (1–17 nmol, ~1 h prior to imaging), and Qtracker 800 (20 pmol, 1 h prior to imaging) from the Qtracker 800 cell labeling kit (Invitrogen, Carlsbad, California). Mice were imaged at multiple time points before and after administration of fluorophores in planar fluorescence mode with 750-nm excitation and in transmission geometry for multiple SD pairs at the excitation wavelength (750-nm excitation, 716/40-nm or 750/10-nm BP filters) and emission wavelength (800-nm LP filter).

3 Results

3.1 *In Vivo Lifetime Characteristics of Commercial Fluorophores*

Lifetime multiplexing assumes that each fluorophore present has a characteristic lifetime decay *in vivo*. The variety of chemical environments encountered *in vivo* could potentially cause a single fluorophore to exhibit a range of lifetimes across the mouse, as described for some probes.[6,18] This could complicate multiplexing, because of the loss of lifetime-based specificity.

However, for a number of commercially available probes, we observe narrow *in vivo* lifetime distributions (Fig. 1). With intravenous administration, these fluorophores have surface temporal decays that are well fit with a monoexponential model, and lifetime distributions that have little variance across the mouse. Lifetimes for the different dyes range from 616 to 1343 ps (Table 1). Some fluorophores undergo characteristic lifetime changes during normal biodistribution and pharmacokinetics. Kodak X-Sight 761 exhibits lifetime short-

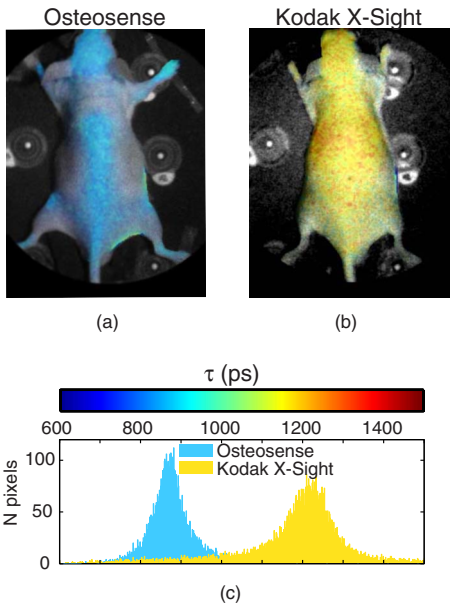

Fig. 1 *In vivo* lifetime characteristics of commercially available NIR fluorophores. Mice were administered NIR fluorophores and imaged for up to 1 day to determine biodistribution and *in vivo* fluorescence lifetimes. Planar fluorescence images were thresholded and each pixel was fit for a monoexponential decay. Monoexponential lifetime maps for (a) Osteosense and (b) Kodak X-Sight 761, overlaid on a white light planar reflectance image of the mouse. (c) Histogram of pixel lifetime values from (a) and (b). The two fluorophores have distinct, separable lifetimes *in vivo*.

Table 1 Lifetime characteristics of commercial NIR fluorophores. Emission wavelengths are taken from product literature. Mean lifetime ± the standard deviation are derived from monoexponential fit of images taken at time points from 1 min to 24 h following fluorophore injection with the mouse supine or prone, depending on the organs of interest. Only pixels with peak intensity >10% of the maximum intensity were considered in the fit (to avoid low-intensity noisy pixels). The standard deviation for all pixels was ~2 to 3× the values listed here. $\tau\pm$(ps) for Kodak X-Sight 761 shows lifetime shortening in the liver over 14 h and for Atto 740 lifetimes in the kidneys and bladder, respectively. Alexa 750 is antibody conjugated.

Fluorophore	λ_{em} (nm)	$\tau\pm$(ps)
Indocyanine green	835	700±18
Osteosense 750	780	835±47
Kodak X-Sight 761	789	1343±30–1158±12*
IRDye 800	794	906±23
Genhance 750	775	1007±23
Atto 740	764	1130±54, 1003±63†
Alexa 750‡	779	616±26

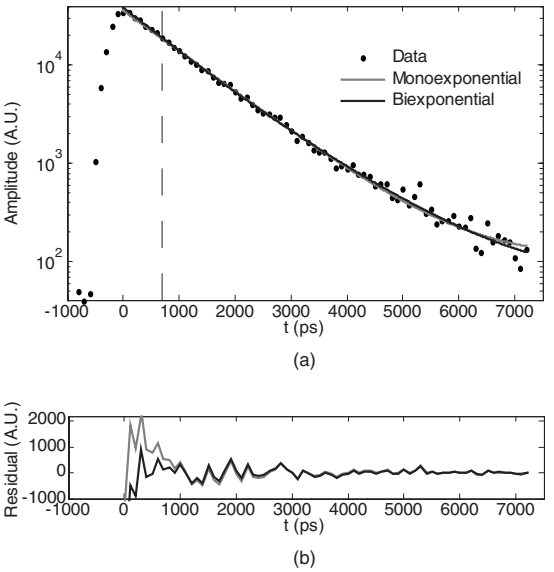

Fig. 2 Mono- versus biexponential analysis. (a) A single pixel data point from an *in vivo* measurement of two fluorophores (Osteosense 750 and Kodak X-Sight 761) was fit for either a single lifetime (monoexponential, resultant τ=1054) or for two *a-priori* lifetimes (biexponential, τ_1=835 ps and τ_2=1343). All data points after the dashed line (representing the time gate for fitting t_d) were included in the fit. (b) Residuals from fits in (a).

ening when accumulating in the liver (from 1343 to 1158 ps over 24 h). Atto 740 has a long lifetime in the kidneys (1130 ps), but shortens when accumulating in the bladder (1003 ps) or when excreted in the bile to the gastrointestinal (GI) tract (1092 ps). Most probes that are cleared via the kidneys undergo similar lifetime shortening in the bladder, as described by other groups.[19]

In summary, a number of commercial NIR fluorophores have lifetime properties *in vivo*, conducive to lifetime-based multiplexing. Lifetime characteristics for these probes are relatively uniform across the entire animal and can be easily determined in advance.

3.2 *Single Versus Multiexponential Analysis*

When two or more fluorophores are present simultaneously, the measured fluorescence is a sum of photons from the respective fluorophores. Monoexponential analysis (e.g., fitting with a monoexponential function) of a mixed signal provides an average lifetime for each detector or pixel, but can be misleading, given the contribution of the fluorophores at different concentrations and quantum efficiencies (see Fig. 2). In contrast, a multiexponential analysis based on expected lifetime components can produce a quantitative measure of multiple fluorophores. Moreover, a monoexponential analysis does not exploit the full power of lifetime-based tomographic separability as afforded by Eq. (2).

As an example, consider multiplexing Osteosense 750, a bone-targeted probe, with Kodak X-Sight 761, which remains in the blood stream and accumulates slowly in the liver. When just Osteosense 750 is present in the animal, the monoexponential lifetime map exhibits a narrow lifetime distribution with mean τ=835 ps [Fig. 3(b)]. Administration of Kodak X-Sight results in a lifetime map with a large distribution of lifetimes, ranging from 1000 to 1500 ps [Fig. 3(g)]. The average lifetime at bony structures is significantly higher than with Osteosense alone, due to the contribution of vascular Kodak X-Sight. Biexponential fitting using average lifetimes for Osteosense (τ=835 ps) and Kodak X-Sight (τ=1343 ps) components results in clear anatomical separation of the two probes [Figs. 3(c)–3(e) and 3(h)–3(j)]. The Osteosense components before and after Kodak X-Sight administration are qualitatively similar [compare Figs. 3(c) and 3(h)] and no Kodak X-Sight is detected by the biexponential fit before administration [Fig. 3(d)].

3.3 *Noise Considerations for Lifetime Multiplexing*

It is clear from Fig. 3 that the amplitude images recovered from lifetime unmixing are influenced by noise. The effect of measurement noise is an uncertainty in the recovered decay amplitudes, which can be quantified by the variance, σ_a^2. This uncertainty depends on both the measurement noise and the separation ($\Delta\tau$) of the lifetimes involved. To estimate σ_a, we analyze the propagation of noise from the measurement (time domain image) to the recovered amplitudes using linear regression theory.[20] The time-dependent measurement $\mathbf{y}$ is linearly related to the amplitudes of the individual decay components decay as $\mathbf{y}=\mathbf{X}\ \mathbf{a}$, where the columns of $\mathbf{X}$ are the normalized, time-dependent monoexponential decays and $\mathbf{a}$ are the component amplitudes. The uncertainty in the recovered amplitudes $\sigma_\mathbf{a}$ is dependent on the measurement noise at each time point, expressed as the weight matrix $\mathbf{W}$, where $\mathbf{W}_{ii}=1/\sigma_{yi}^2$, and the respective basis functions $\mathbf{X}$:

$$\sigma_{aj}^2=[(\mathbf{X}^T\ \mathbf{W}\ \mathbf{X})^{-1}]_{jj}. \tag{3}$$

Equation (3) allows calculation of recovered amplitude uncertainty given known system noise parameters, which determine $\mathbf{W}$, and fluorophore lifetimes, which dictate the basis functions $\mathbf{X}$. Simulations with Eq. (3) show that, as expected, amplitude uncertainty increases as the lifetime separation between probes $\Delta\tau$ decreases [Fig. 4(a)]. For a given lifetime separation, the relative amplitude uncertainty (σ_a/a) for one component increases as the amplitude of the other component increases [Fig. 4(b)]. Practically, this means that if one component is much weaker than the other (Note that the decay amplitude is the product of fluorophore concentration and extinction coefficient.), it will have increased relative uncertainty. Fluorophore separability, defined arbitrarily as the conditions under which relative uncertainty is $<$30%, can be estimated directly as described before. For example, assuming one fluorophore with lifetime τ_1=1000 ps, quantitative unmixing is possible for $\Delta\tau\geqslant$200 ps at relative concentrations as low as 1:5 [Fig. 4(b)].

These observations are corroborated experimentally with Osteosense and Kodak X-Sight in 5% albumin solution, $\Delta\tau\approx$250 ps, mixed at varying concentrations in a multiwell plate (Fig. 5). Amplitude uncertainty is estimated from the recovered amplitude sample uncertainty s_i (an approximation to σ_a). Recovered amplitudes are linear in concentration with $R^2>0.95$. For the imaging specifications typically used in our system, the relative amplitude uncertainty ($s_i/a_i\times100\%$) is $<$50% at concentrations ranging from 200 to 1000 nM (Fig. 5), and $<$30% for all concentrations except 200-nM Osteo-

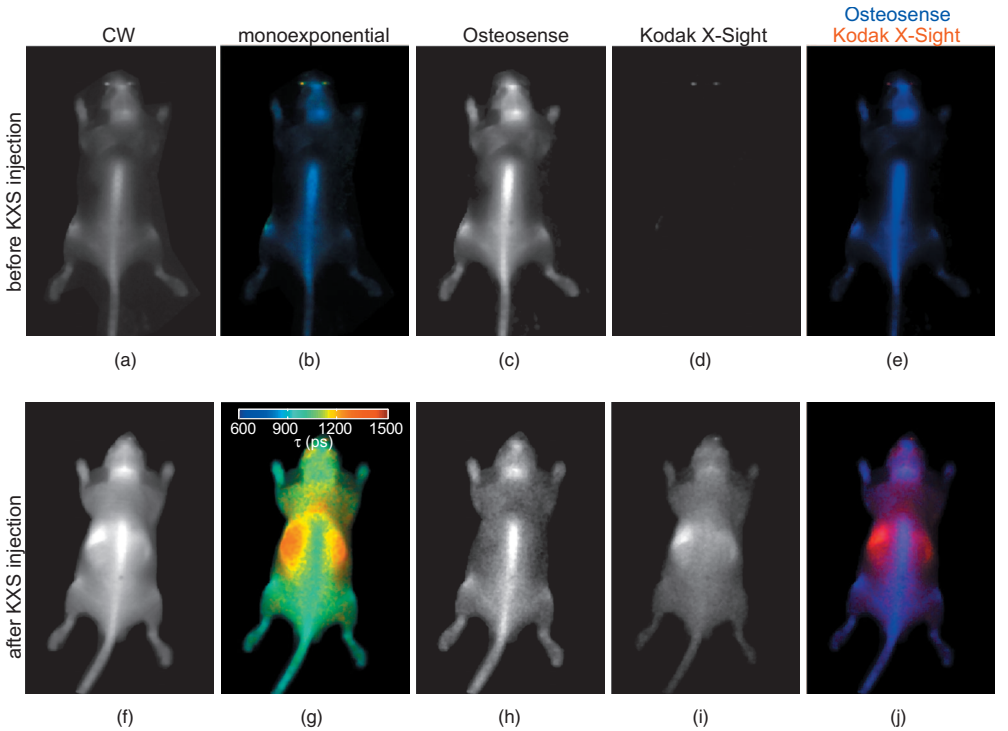

Fig. 3 Planar fluorescence lifetime imaging of Osteosense 750 and Kodak X-Sight 761. A nude mouse received 2-nmol Osteosense 24 h prior to imaging; planar fluorescence time-resolved images were collected immediately before [(a) through (e)] and after [(f) to (j)] administration of Kodak X-Sight 761 (3 nmol). Image pixels were fit for the amplitude and lifetime of a monoexponential function, or were fit for a biexponential function with known lifetime components (see Fig. 2). (a) and (f) Continuous wave (cw) images. (b) and (g) Lifetime maps from monoexponential fit; color bar indicates the lifetime colormap. (c) and (h) Osteosense 750 lifetime component (τ_1=835 ps) from biexponential fit. (d) and (i) Kodak X-Sight 761 lifetime component (τ_2=1343 ps). (e) and (j) RGB images with Osteosense component in blue and Kodak X-Sight in red.

sense with 800 to 1000-nM Kodak X-Sight. The amplitude uncertainty s_i is highest for high amplitude signals, regardless of which fluorophore is contributing more photons to the mixed signal. Under conditions where one fluorophore is at a low concentration relative to the other, the low concentration dye has the lowest signal-to-noise ratio and therefore the highest relative amplitude uncertainty.

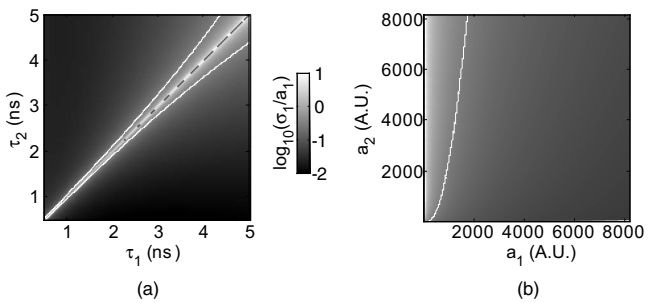

Fig. 4 Noise considerations for lifetime unmixing. Lifetime recovery was simulated assuming Poisson statistics, i.e., $\sigma_y^2=\beta y+\sigma_r^2$,[13] with β =6.53 and a dynamic range of 2^{14} (4×4 hardware and 2×2 software binning). (a) Relative amplitude uncertainty for equal amplitude probes of lifetimes τ_1 and τ_2. (b) Relative amplitude uncertainty of the first amplitude component for varying amplitudes a_1 and a_2 over the dynamic range of the instrument, with fixed lifetimes τ_1=1 ns and τ_2=1.2 ns. The white lines in (a) and (b) indicate the 30% relative uncertainty contours.

Measurement noise also affects the determination of the lifetime τ from a monoexponential fit, e.g., when measuring the *in vivo* lifetime characteristics of a fluorophore. We estimated the propagation of measurement noise by simulating a fluorophore that has a fixed τ and realistic amplitude distribution (chosen from the mean lifetime and amplitude distribution of a similar *in vivo* measurement), and noise according to a conservative empirical model; the simulated measurement is then fit at each pixel for τ. As shown in Fig. 6, the uncertainty in τ due to noise is ~20%, which accounts for the majority of the *in vivo* lifetime heterogeneity observed in this study, and provides a qualitative explanation for the limits on fluorophores unmixing (described before). Finally, measurement noise sets a limit on the number of fluorophores that can be multiplexed. Figure 7 shows the amplitude uncertainty with a simulation of lifetime multiplexing using up to five lifetimes with the shot noise model. This indicates that under the noise statistics used here, the maximum number of fluorphores that can be multiplexed reasonably (less than 30% relative uncertainty) is three.

3.4 *Tomography of Multiple Fluorophores*

We demonstrate tomographic lifetime multiplexing (described in Sec. 2) for two and three anatomically targeted fluorophores injected in living mice. As a first example, we image Kodak X-Sight and Osteosense in nude mice (n=3), with a time-resolved, limited angle, free-space tomographic imaging

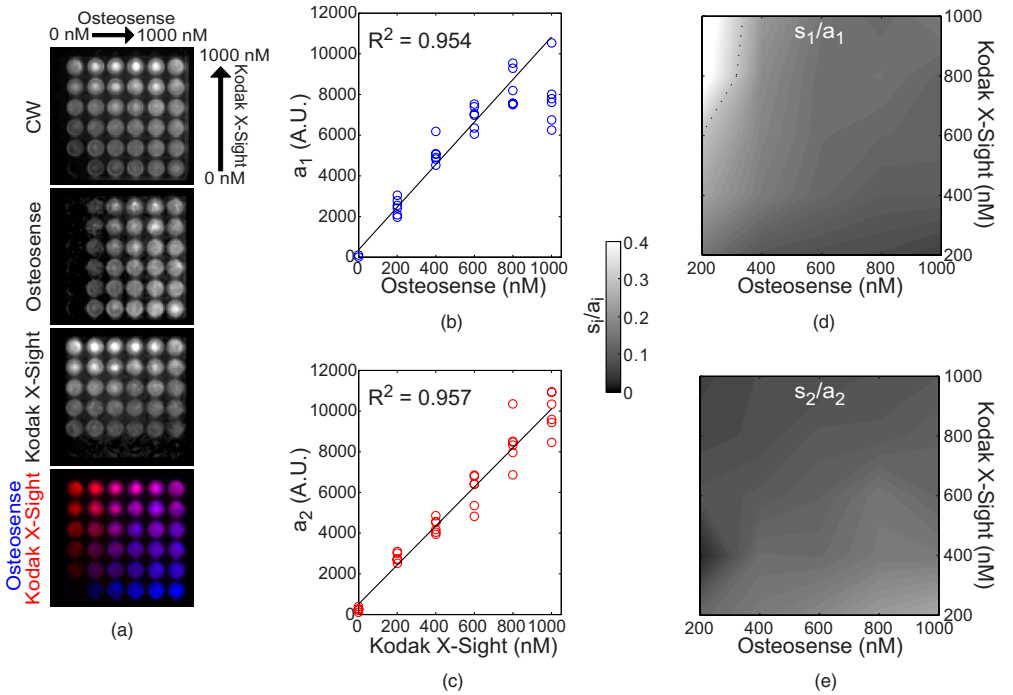

Fig. 5 Multiwell separation of Osteosense and Kodak X-Sight. A multiwell plate was filled with Osteosense and Kodak X-Sight in orthogonal axes, from 0 to 1000 nM, in 200-nM steps. The multiwell plate was imaged in planar fluorescence mode, and subsequent images were fit for the lifetime components of 1126 (a_1, Osteosense) and 1376 ps (a_2, Kodak X-Sight), which were obtained from wells containing only a single fluorophore. (a) cw and recovered amplitude components of the multiwell plate. In the biexponential frame (bottom), Kodak X-Sight is in red, Osteosense is in blue. (b) and (c) Recovered component amplitudes (arbitrary units, AU) and linear fit to fluorophore concentration; correlation is shown in top left of each graph. (d) and (e) Amplitude uncertainty (s_i/a_i), for (d) Osteosense and (e) Kodak X-Sight. (Color online only.)

system.[12] Excitation and fluorescence measurements are collected from a grid of sources and detectors (~3×3-mm separation) 1 h after Kodak X-Sight administration and >24 h after Osteosense administration [Fig. 8(b)]; at these time points, the two probes are localized to specific organs (liver and bones, respectively) with characteristic lifetimes and little off-site accumulation. Individual measurements are fit for two exponentials (τ_1=835 ps and τ_2=1242 ps) and display a fluorophore-specific distribution [Fig. 8(e)]. Note that the scale for the Kodak X-Sight amplitude component is ~5-fold greater than the Osteosense amplitude scale.

At this time point (1 h after Kodak X-Sight administration) on planar fluorescence images, Osteosense is confined to bony structures, including the spinal column, pelvis, skull, and long bones, whereas Kodak X-Sight has localized to the liver, with residual Kodak X-Sight in the vascular compartment [Figs. 8(c) and 8(d)]. This observation is consistent with previous biodistribution studies of the respective fluorophores alone. Lifetime-based 3-D reconstructions corroborate the planar fluorescence images: Kodak X-Sight is observed in the

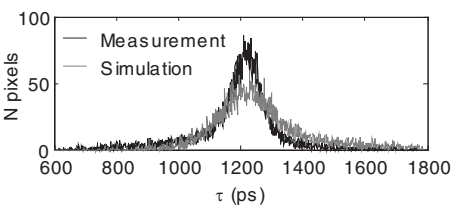

Fig. 6 Noise propagation to τ. The effects of measurement noise on the estimation of τ were determined by simulating a measurement of Kodak X-Sight *in vivo* using the mean lifetime and amplitude distribution of an actual Kodak X-Sight measurement (shown in Fig. 1). We added noise according to our empirical noise model, with β=6.53; each pixel was fit for τ and then plotted as a histogram. The measurement is shown above in black and the simulation in gray. The standard deviation for the measurement was 157 and the simulation was 193, which reflects the conservative noise model (adds slightly more noise than needed).

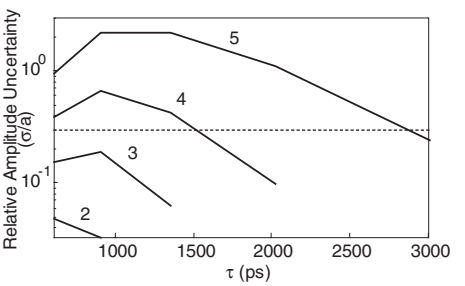

Fig. 7 Uncertainty for multiple components. The limitations of additional components were tested by simulating n=2 to 5 lifetimes, with the initial lifetime τ_1=600 ps and each additional lifetime 1.5× the previous; amplitudes were split evenly between the components as 4096×4/n. Noise was added according to the conservative noise model for 4×4 hardware binning and 2×2 software binning. The relative uncertainty was calculated for each lifetime component as additional components were added. The 30% uncertainty cutoff is shown as a dotted line.

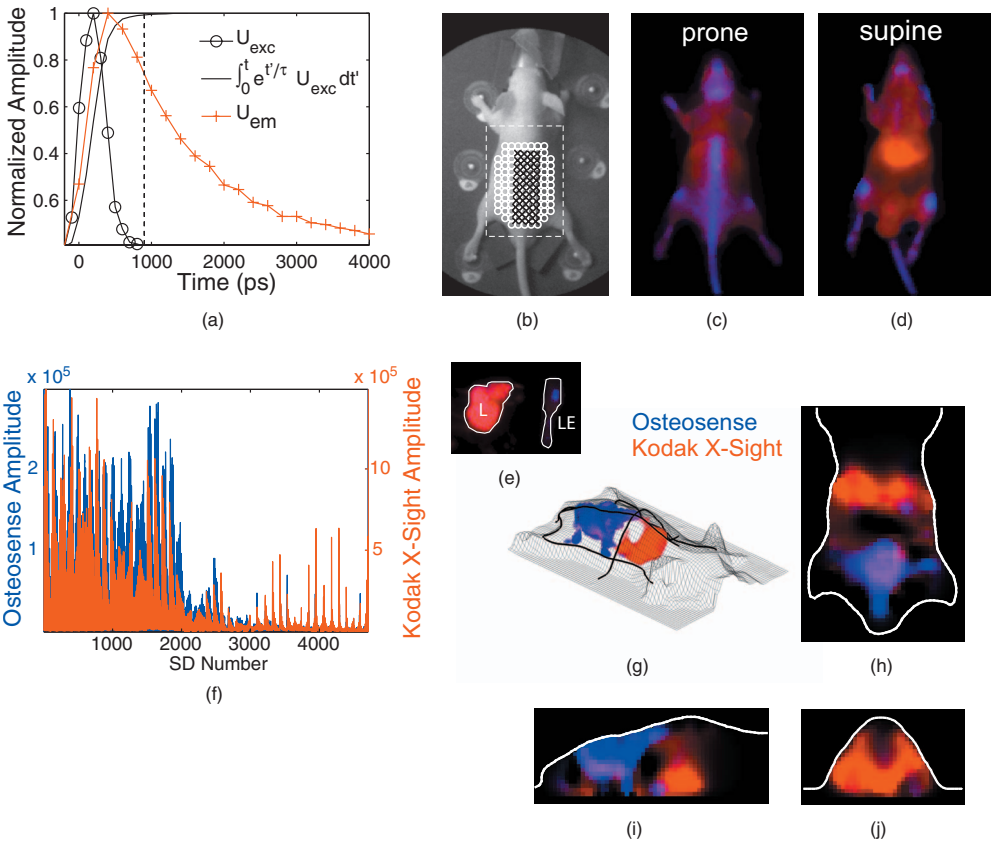

Fig. 8 Tomography of two fluorophores. Nude mice were administered Osteosense (24 h prior) and Kodak X-Sight (1 h prior) and imaged with time-resolved planar fluorescence and tomography. Tomographic reconstructions used excitation (750/40-nm BP filter), emission (800-nm LP filter), and surface topography measurements, for 44 sources and 107 detectors. (a) Representative time-resolved data for tomographic reconstructions. The product of the excitation measurement (U_{exc}) and the fluorophore exponential was integrated over time ($\int_0^t e^{(t')/\tau} U_{exc} dt'$), and all time points after 99% of the max (dashed line) were used for lifetime fitting. (b) White light planar reflectance image with source (black "x") and detector locations (white "o"). The reconstructed volume is indicated with the dashed white box. (c) through (e) Unmixed planar fluorescence images with Osteosense (blue) and Kodak X-Sight (red). Postmortem organs (liver L; amputated lower extremity LE) are shown in (e). (f) Recovered amplitude components for 44×107 SD pairs. (g) 3-D rendering of surface (grid) and the Osteosense and Kodak X-Sight distributions. The location of slices in (g) through (h) is shown in bold black lines. (h) through (j) Slices from lifetime-separated reconstruction. Surface boundaries are indicated in white.

liver region [Figs. 8(f)–8(i)] and Osteosense is localized to the pelvis and the back. These findings were confirmed by postmortem imaging of the organs and bones. Thus, the two lifetime components are regionally distinct and correctly localized.

3-D reconstructions exhibit some plume artifacts, especially in the z axis. In addition, Osteosense is not detected at the highest point of the spinal column, above the liver and thoracic cavity, due to the low transmission across those structures. These effects may be attributed to the limited-angle measurement scheme employed by our system, and primarily impact the Osteosense reconstruction because of its anatomical distribution.

Lifetime multiplexing can be extended to more than two fluorophores. As an example, we image Qtracker 800, a quantum dot with an extremely long lifetime, in addition to Atto 740 (τ=1092 ps at 1-h postinjection) and Osteosense 750. Because it is much longer than the pulse repetition frequency of our laser, the Qtracker lifetime can be approximated as the DC component a_o in Eq. (1). The three fluorophores have distinct biodistributions and anatomical targets: Atto 740 is cleared via the liver and secreted with the bile to the gastrointestinal tract; after 1 h, Atto is localized to the duodenum. Qtracker (from the cell labeling kit) is cleared immediately by the liver, and remains stable there for >24 h.

When imaged together, there is distinct localization of the three fluorophores. Qtracker is resolved primarily in the liver, Osteosense in the bony structures, and Atto in the proximal small bowel, localized to the right upper quadrant (Fig. 9). These locations match surface fluorescence images and postmortem imaging. Surface and tomographic images are obtained with Atto and Osteosense components ~100-fold greater than the Qtracker component, and for a relatively small difference in lifetime for the organic compounds ($\Delta\tau \approx 250$ ps).

4 Discussion

Lifetime-based multiplexing enables simultaneous imaging of multiple fluorophores. This simple approach overcomes the spectral bandwidth limitations of the NIR regime, and in contrast to frequency domain (FD),[21] monoexponential analysis,[6]

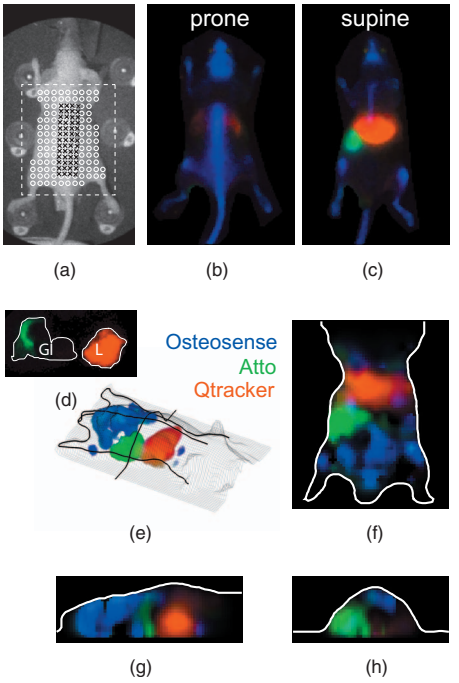

Fig. 9 Tomography of three fluorophores. Nude mice received Osteosense (24 h prior), Atto 740 (1.25 h prior), and Qtracker 800 (1 h prior), and were imaged using planar fluorescence and tomography. (a) White light planar reflectance image with source (black "x") and detector locations (white "o"). The reconstructed volume is indicated with the dashed white box. (b) through (d) Unmixed planar fluorescence images with Osteosense (blue, labels bones), Atto (green, localized to proximal small bowel), and Qtracker (red, localized to the liver). Postmortem organs (gastrointestinal tract, removed *en bloc*, GI; liver, L) are shown in (d). The Atto signal is confined to the proximal small bowel. (e) 3-D representation of three fluorophores within the surface boundaries (mesh grid). The location of planes in (f), (g), and (h) are shown in bold black. (f), (g), and (h) Slices from lifetime-separated reconstruction. Surface boundaries are indicated in white.

forward Laplace,[22,23] or moment-based approaches,[24] determines fluorophore concentrations directly from the time-domain signal without the need for additional data processing. Unmixed amplitudes are linear with fluorophore concentration (Fig. 5) and can be input directly into the inversion equation for 3-D reconstructions.

Lifetime multiplexing should be generalizable to the full NIRF probe repertoire, after proper *a-priori* characterization of *in vivo* fluorophore decay characteristics. The commercial fluorophores we tested have narrowly distributed, monoexponential lifetimes and are therefore suitable for *in vivo* multiplexing (Table 1). It is expected that antibody-conjugated probes would exhibit similar *in vivo* lifetime characteristics. From simulations and experiments, we expect that any two fluorophores that differ by ~20% could be imaged together; for example, any of the short-lifetime probes tested (indocyanine green, Osteosense 750, and Alexa 750) could be multiplexed with the long-lifetime probes (Kodak X-Sight 761 and Atto 740).

The separability of a given dye pair can be determined directly from the lifetimes and imaging system noise. For our system, quantitative unmixing of multiple fluorophores is not possible for $\Delta\tau < 200$ ps at lifetimes around 1000 ps; above 200 ps, unmixing is possible with better than 30% amplitude uncertainty for relative fluorophore concentrations of at least 1:5 (Figs. 4 and 5). This limit in $\Delta\tau$ can at least qualitatively be explained by noise propagation from the image to τ: simulations show that the standard deviation in τ is ~20%. Thus, asymptotic lifetime separation, as described in this study, is noise limited and therefore system dependent.

Some have suggested that because asymptotic fitting includes noisy data points from the "tail" of the fluorescence decay, it is inherently disadvantaged compared to cw imaging. However, this is at least partially alleviated by increasing the CCD exposure time to achieve detector saturation at the earliest portion of the asymptotic regime, and by weighting the lifetime fit with the measurement variance. For fluorophores with large lifetime separation, the amplitude variance approaches the measurement noise, and thus is comparable to cw measurement noise, but with the benefit of multiplexing.

Although monoexponential probes are desirable, more complicated fluorophores could be imaged with multiexponential fits (assuming *a-priori* lifetimes). In the case of a fluorophore with a distinct lifetime when accumulated at the target,[6] two lifetimes could be used in a multiexponential fit to produce separate images of target-bound and unbound probes. With more complicated decay functions, such as autofluorescence, it may be possible to approximate fluorophore decays with multi-or stretched exponential basis functions,[25] although calculation of the tomography forward problem in these cases may be more difficult. We conclude that most, if not all, NIR fluorophores could be used for lifetime-based tomographic multiplexing.

In this study, we extended lifetime multiplexing to 3-D tomography using a theory developed previously.[7] We imaged *in vivo* in nude mice with two and three fluorophores that localized to distinct anatomical targets, as confirmed by postmortem imaging (Figs. 8 and 9). Lifetime-separated reconstructions corresponded well to unmixed 2-D planar images and known organ locations.

Tomographic reconstruction also has limitations inherent to measurement geometry and light diffusion physics. The reconstructions presented here are prone to poor z-axis resolution and full-thickness penetration in the thorax because of the limited-angle configuration of our tomographic imaging system. More sophisticated, full 360-deg measurement schemes have somewhat alleviated these issues for cw tomography.[26] We anticipate that integration of time-resolved measurement into a full rotational tomography system will enable better z-axis resolution and penetration in highly absorbing regions.

Lifetime-based NIRF multiplexed tomography is a powerful technique that should allow translation of other lifetime-based methods to 3-D imaging. Fluorescence lifetime is sensitive to FRET between donor and acceptor fluorophores,[27] and thereby may enable tomographic imaging of protein interactions throughout the mouse. Furthermore, fluorophores can be designed to exhibit lifetime shifts upon target binding;[28] with lifetime multiplexing, signals from the unbound probe (due to imperfect uptake) could be effectively removed, resulting in improved signal-to-noise reconstructions of the target-bound probe. Probes with two distinct lifetime states (ligand bound versus unbound) also offer the pos-

sibility of quantitative measurements of ligand concentration. For example, visible fluorescent Ca^{2+} sensors have been used to measure absolute calcium concentrations in solution and *in vivo*.[29,30] The success of these future applications will depend primarily on the development of NIR analogs to existing visible fluorophore sensors.

In summary, we have demonstrated a new technique for tomographic imaging of multiple fluorophores in small animals. Our lifetime-based approach uses *a-priori* information about fluorophore decay characteristics to separate a fluorophore's distinct signal from that of others. Once unmixed, the signal can be directly input into the tomography inverse problem, resulting in multiplexed 3-D reconstructions. Asymptotic lifetime separation is possible for fluorophores with even small lifetime differences and for many fluorophores at once. We anticipate that lifetime-based NIRF tomography will be a powerful tool for molecular imaging in the future.

Acknowledgments

This research was supported by NIH EB000768 and AG026240. Raymond was supported by NIH T32 EB001680.

References

1. G. Gaietta, T. J. Deerinck, S. R. Adams, J. Bouwer, O. Tour, D. W. Laird, G. E. Sosinsky, R. Y. Tsien, and M. H. Ellisman, "Multicolor and electron microscopic imaging of connexin trafficking," *Science* **296**, 503–507 (2002).
2. B. J. Bacskai, S. T. Kajdasz, R. H. Christie, C. Carter, D. Games, P. Seubert, D. Schenk, and B. T. Hyman, "Imaging of amyloid-beta deposits in brains of living mice permits direct observation of clearance of plaques with immunotherapy," *Nat. Med.* **7**, 369–372 (2001).
3. B. Huang, S. A. Jones, B. Brandenburg, and X. Zhuang, "Whole-cell 3d storm reveals interactions between cellular structures with nanometer-scale resolution," *Nat. Methods* **5**, 1047–1052 (2008).
4. X. Gao, Y. Cui, R. M. Levenson, L. W. Chung, and S. Nie, "In vivo cancer targeting and imaging with semiconductor quantum dots," *Nat. Biotechnol.* **22**, 969–976 (2004).
5. S. V. Patwardhan and J. P. Culver, "Quantitative diffuse optical tomography for small animals using an ultrafast gated image intensifier," *J. Biomed. Opt.* **13**, 011009 (2008).
6. S. Bloch, F. Lesage, L. McIntosh, A. Gandjbakhche, K. Liang, and S. Achilefu, "Whole-body fluorescence lifetime imaging of a tumor-targeted near-infrared molecular probe in mice," *J. Biomed. Opt.* **10**, 054003 (2005).
7. A. T. N. Kumar, J. Skoch, B. J. Bacskai, D. A. Boas, and A. K. Dunn, "Fluorescence-lifetime-based tomography for turbid media," *Opt. Lett.* **30**, 3347–3349 (2005).
8. W. Akers, F. Lesage, D. Holten, and S. Achilefu, "In vivo resolution of multiexponential decays of multiple near-infrared molecular probes by fluorescence lifetime-gated whole-body time-resolved diffuse optical imaging," *Mol. Imaging* **6**, 237–246 (2007).
9. C. D. Salthouse, F. Reynolds, J. M. Tam, L. Josephson, and U. Mahmood, "Quantitative measurement of protease activity with correction of probe delivery and tissue absorption effects," *Sens. Actuators B* **138**, 591–597 (2009).
10. D. J. Hall, U. Sunar, S. Farshchi-Heydari, and S. H. Han, "In vivo simultaneous monitoring of two fluorophores with lifetime contrast using a full-field time domain system," *Appl. Opt.* **48**, D74–D78 (2009).
11. A. T. N. Kumar, S. B. Raymond, G. Boverman, D. A. Boas, and B. J. Bacskai, "Time resolved fluorescence tomography of turbid media based on lifetime contrast," *Opt. Express* **14**, 12255–12270 (2006).
12. A. T. N. Kumar, S. B. Raymond, A. K. Dunn, B. J. Bacskai, and D. A. Boas, "A time domain fluorescence tomography system for small animal imaging," *IEEE Trans. Med. Imaging* **27**, 1152–1163 (2008).
13. D. Hyde, E. Miller, D. H. Brooks, and V. Ntziachristos, "A statistical approach to inverting the born ratio," *IEEE Trans. Med. Imaging* **26**, 893–905 (2007).
14. D. A. Boas, J. P. Culver, J. J. Stott, and A. K. Dunn, "Three dimensional monte carlo code for photon migration through complex heterogeneous media including the adult human head," *Opt. Express* **10**, 159–170 (2002).
15. D. A. Boas, T. Gaudette, and S. R. Arridge, "Simultaneous imaging and optode calibration with diffuse optical tomography," *Opt. Express* **8**, 263–270 (2001).
16. P. K. Yalavarthy, B. W. Pogue, H. Dehghani, and K. D. Paulsen, "Weight-matrix structured regularization provides optimal generalized least-squares estimate in diffuse optical tomography," *Med. Phys.* **34**, 2085–2098 (2007).
17. W. J. Akers, M. Y. Berezin, H. Lee, and S. Achilefu, "Predicting in vivo fluorescence lifetime behavior of near-infrared fluorescent contrast agents using in vitro measurements," *J. Biomed. Opt.* **13**, 054042 (2008).
18. M. Hassan, J. Riley, V. Chernomordik, P. Smith, R. Pursley, S. B. Lee, J. Capala, and A. H. Gandjbakhche, "Fluorescence lifetime imaging system for in vivo studies," *Mol. Imaging* **6**, 229–236 (2007).
19. R. J. Goiffon, W. J. Akers, M. Y. Berezin, H. Lee, and S. Achilefu, "Dynamic noninvasive monitoring of renal function in vivo by fluorescence lifetime imaging," *J. Biomed. Opt.* **14**, 020501 (2009).
20. W. H. Press, S. A. Teukolsky, W. T. Vetterling, and B. P. Flannery, *Numerical Recipes in C: the Art of Scientific Computing*, 2nd ed., Cambridge University Press, New York (1992).
21. R. E. Nothdurft, S. V. Patwardhan, W. Akers, Y. Ye, S. Achilefu, and J. P. Culver, "In vivo fluorescence lifetime tomography," *J. Biomed. Opt.* **14**, 024004 (2009).
22. J. Wu, L. Perelman, R. R. Dasari, and M. S. Feld, "Fluorescence tomographic imaging in turbid media using early-arriving photons and laplace transforms," *Proc. Natl. Acad. Sci. U.S.A.* **94**, 8783 (1997).
23. F. Gao, H. Zhao, Y. Tanikawa, and Y. Yamada, "A linear, featured-data scheme for image reconstruction in time domain fluorescence molecular tomography," *Opt. Express* **14**, 7109–7124 (2006).
24. S. Lam, F. Lesage, and X. Intes, "Time domain fluorescent diffuse optical tomography: analytical expressions," *Opt. Express* **13**, 2263–2275 (2005).
25. A. T. N. Kumar, E. Chung, S. B. Raymond, J. van de Water, K. Shah, R. K. Jain, B. J. Bacskai, and D. A. Boas, "Feasibility of in vivo imaging of fluorescent proteins using lifetime contrast," *Opt. Lett.* **34**, 2066–2068 (2009).
26. N. Deliolanis, T. Lasser, D. Hyde, A. Soubret, J. Ripoll, and V. Ntziachristos, "Free-space fluorescence molecular tomography utilizing 360 degrees geometry projections," *Opt. Lett.* **32**, 382–384 (2007).
27. B. J. Bacskai, J. Skoch, G. A. Hickey, and B. T. Hyman, "Fluorescence resonance energy transfer determinations using multiphoton fluorescence lifetime imaging microscopy to characterize amyloid-beta plaques," *J. Biomed. Opt.* **8**, 368–375 (2003).
28. S. B. Raymond, J. Skoch, I. D. Hills, E. E. Nesterov, T. M. Swager, and B. J. Bacskai, "Smart optical probes for near-infrared fluorescence imaging of alzheimer's disease pathology," *Eur. J. Nucl. Med. Mol. Imaging* **35**, 1032–1032 (2008).
29. C. D. Wilms and J. Eilers, "Photo-physical properties of ca2+-indicator dyes suitable for two-photon fluorescence-lifetime recordings," *J. Microsc.* **225**, 209–213 (Mar 2007).
30. K. V. Kuchibhotla, C. R. Lattarulo, B. T. Hyman, and B. J. Bacskai, "Synchronous hyperactivity and intercellular calcium waves in astrocytes in alzheimer mice," *Science* **323**, 1211–1215 (2009).